RESEARCH ARTICLE
doi: 10.2306/scienceasia1513-1874.2024.100

ScienceAsia 50 (6): 2024: ID 2024100: **1–10**

New analytical function of potential and fast algorithm for solving potentials in $m \times n$ fan resistor network

Gaojun Zhang[a], **Xiaoyu Jiang**[a,*], **Yanpeng Zheng**[b,*], **Zhaolin Jiang**[c]

[a] School of Information Science and Engineering, Linyi University, Linyi 276000 China
[b] School of Automation and Electrical Engineering Linyi University, Linyi 276000 China
[c] School of Mathematics and Statistics, Linyi University, Linyi 276000 China

*Corresponding authors, e-mail: jxy19890422@sina.com, zhengyanpeng0702@sina.com

Received 18 Jul 2023, Accepted 30 Sep 2024
Available online 30 Nov 2024

ABSTRACT: This paper presents a refined analytical potential function (APF) for the $m \times n$ fan resistor network. Firstly, the original piecewise APFs are replaced with a single analytic function, which improves the calculation scalability. Secondly, Chebyshev polynomials of the second class are introduced to represent the analytical function of potential. A fast algorithm for calculating potentials is then developed using the sixth type of discrete sine transform, significantly reducing the computation time required for potential calculations. The paper simultaneously solves the APFs for several special cases, presenting their potentials in three-dimensional views. Finally, experiments are conducted to analyze the time and scalability of different methods for calculating the potential. The results of these experiments demonstrate that the improved potential function and fast algorithm enable efficient manipulation of large-scale resistor networks, the application scale of the original APF has been expanded.

KEYWORDS: resistor network, potential, fast algorithm

MSC2020: 15A18 31C20 65Y20

INTRODUCTION

Since the advent of modern science, numerous complex challenges have arisen across various fields, including physics, materials science, and computer science. To tackle these issues, researchers have explored various methodologies. Extensive research has demonstrated that resistor network models [1–6] can directly or indirectly solve many of these problems. The study of resistor networks has yielded numerous significant findings, encompassing theories related to electromigration, impedance networks, and Laplace's method for resistor networks [5–10]. In recent years, Tan [11–17] has introduced the recursive transformation (RT) method as a simpler alternative to the Laplace matrix method for solving explicit functions of potential in resistor networks. Additionally, computer-based approaches are increasingly employed to efficiently and extensively calculate the potential of certain resistor networks [18–22].

Tan [23] innovatively constructed the mathematical model of a fan resistor network with arbitrary boundary resistances. Based on this model, the unparalleled analytical potential function (APF) was obtained theoretically. Everything would be transformed if computer analysis and application of physical functions and mathematical models were employed. Therefore, in order to better adapt to computer analysis, optimizing the theoretically perfect APFs, is a commendable idea aimed at improving the efficiency in calculating potential. In order to enhance the computational efficiency and scale of the analytic potential function, this study re-represents the original segmented analytic potential function using the second-kind Chebyshev polynomials (CPs) and absolute value function, thereby improving the computational performance of the analytic potential function. At the same time, a fast algorithm that can efficiently calculate the potential value of a large-scale resistor network is created.

In 2018, Tan proposed an $m \times n$ fan network with arbitrary boundary resistances [23]. The network is illustrated in Fig. 1a and Fig. 1b, where $m = 10$ and $n = 8$ denote the number of resistors on the meridian and latitude lines, respectively. The resistors on the left and right boundaries are represented by r_1 and r_2. In contrast, the resistors on the other meridians are denoted by r_0, and the resistors on the latitude lines are denoted by r. Moreover, $d(x, y)$ represents each node in the network, where $O(0, 0)$ is defined as the origin and $U(0, 0) = 0$. The input and output points of the current J are denoted as d_1 and d_2, respectively. The potential at any node $d(x, y)$ is given by $U_{m\times n}(x, y)$. The analytical function describing the potential at any node in the resistor network is as follows [23]:

$$\frac{U_{m\times n}(x,y)}{J} = \frac{2r_0}{2m+1}\sum_{i=1}^{m}\left(\frac{\beta^{(i)}_{x_1,x}S_{y_1,i} - \beta^{(i)}_{x_2,x}S_{y_2,i}}{(1-\cos\theta_i)G^{(i)}_n}\right)S_{y,i}, \quad (1)$$

where

$$F^{(i)}_k = (\lambda^k_i - \bar{\lambda}^k_i)/(\lambda_i - \bar{\lambda}_i), \quad \Delta F^{(i)}_k = F^{(i)}_{k+1} - F^{(i)}_k, \quad (2)$$

$$\alpha^{(i)}_{s,x} = \Delta F^{(i)}_x + (b_s - 1)\Delta F^{(i)}_{x-1}, \quad b_s = r_s/r_0, \quad (3)$$

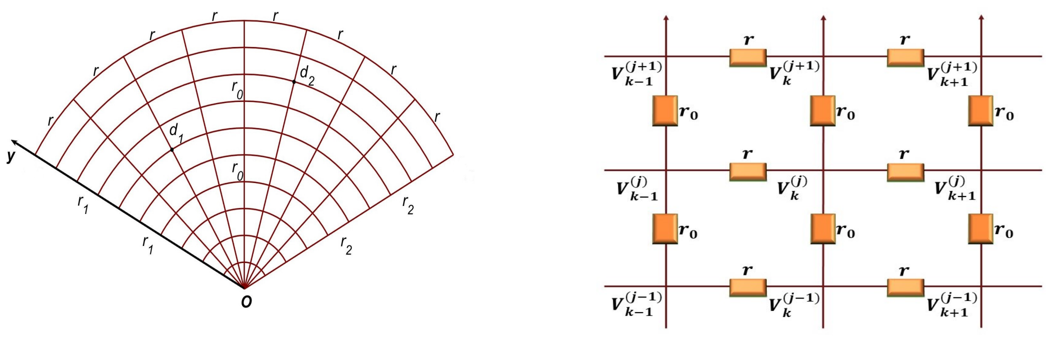

(a) (b)

Fig. 1: (a) The $m\times n$ fan resistor network with arbitrary left and right boundary resistances is considered, where point O serves as the origin. The resistance between any two nodes on each latitude line is denoted as r, with n resistors on each latitude line. Additionally, the resistance between any two nodes on each meridian line is denoted as r_0, with resistances r_1 and r_2 present on the left and right boundaries, respectively. The number of resistors on each meridian line is m. Nodes d_1 and d_2 can represent any arbitrary input and output points for the current J; (b) the part of the fan resistor network, including resistors, node potential, and current direction.

$$\beta_{x_s,x}^{(i)}=\begin{cases}\alpha_{1,x_s}^{(i)}\alpha_{2,n-x}^{(i)}, & \text{if } x\geqslant x_s,\\ \alpha_{1,x}^{(i)}\alpha_{2,n-x_s}^{(i)}, & \text{if } x\leqslant x_s,\end{cases} \tag{4}$$

$$G_n^{(i)}=F_{n+1}^{(i)}+(b_1+b_2-2)F_n^{(i)}+(b_1-1)(b_2-1)F_{n-1}^{(i)}, \tag{5}$$

$$S_{k,i}=\sin(y_k\theta_i),\quad \theta_i=(2i-1)\pi/(2m+1), \tag{6}$$

and

$$\begin{aligned}\lambda_i&=1+b-b\cos\theta_i+\sqrt{(1+b-b\cos\theta_i)^2-1},\\ \bar{\lambda}_i&=1+b-b\cos\theta_i-\sqrt{(1+b-b\cos\theta_i)^2-1}.\end{aligned} \tag{7}$$

The presence of piecewise functions and exponential operations in the APF (1) poses challenges for computing the scale and efficiency of the resistor network. It becomes difficult to achieve fast large-scale numerical operations due to these complexities.

NEW ANALYTICAL FUNCTION OF THE POTENTIAL REPRESENTED BY CHEBYSHEV POLYNOMIALS

In this section, we propose a new analytical function for the potential in the fan resistor network [23], which is represented by a single function using CPs of the second class [24].

Let's consider a scenario where a current J flows in at $d_1(x_1,y_1)$ with $0\leqslant x_1\leqslant n$ and $0\leqslant y_1\leqslant m$, and flows out at $d_2(x_2,y_2)$ with $0\leqslant x_2\leqslant n$ and $0\leqslant y_2\leqslant m$. The new analytical function of potential for the $m\times n$ fan resistor network can be expressed as follows:

$$\begin{aligned}\frac{U_{m\times n}(x,y)}{J}&=\frac{2r_0}{2m+1}\sum_{j=1}^{m}\frac{\Upsilon_{x,x_1}^{(j)}P_{y_1,j}-\Upsilon_{x,x_2}^{(j)}P_{y_2,j}}{(1-\cos\frac{(2j-1)\pi}{2m+1})H_n^{(j)}}P_{y,j}(T_{0.5}^{(j)})^2\\ &=\frac{2r_0}{2m+1}\frac{\langle\Upsilon_{x,x_1},P_{y_1}\rangle-\langle\Upsilon_{x,x_2},P_{y_2}\rangle}{\langle\alpha,H_n\rangle}\langle P_y,T_{0.5}\rangle,\end{aligned} \tag{8}$$

where

$$\Upsilon_{x,x_t}=\left[\Upsilon_{x,x_t}^{(1)},\Upsilon_{x,x_t}^{(2)},\cdots,\Upsilon_{x,x_t}^{(j)},\cdots,\Upsilon_{x,x_t}^{(m)}\right],\quad x_t=x_1,x_2,$$

$$P_k=\left[P_{k,1},P_{k,2},\cdots,P_{k,j},\cdots,P_{k,m}\right],\quad k=y,y_1,y_2,$$

$$T_{0.5}=\left[(T_{0.5}^{(1)})^2,(T_{0.5}^{(2)})^2,\cdots,(T_{0.5}^{(j)})^2,\cdots,(T_{0.5}^{(m)})^2\right],$$

$$\alpha=\Big[(1-\cos\frac{\pi}{2m+1}),(1-\cos\frac{3\pi}{2m+1}),\cdots,(1-\cos\frac{(2j-1)\pi}{2m+1}),\cdots,2\Big],$$

$$H_n=\left[H_n^{(1)},H_n^{(2)},\cdots,H_n^{(j)},\cdots,H_n^{(m)}\right],$$

$$\Upsilon_{x,x_t}^{(j)}=\varsigma_{1,x,x_t}^{(j)}+\varsigma_{2,x,x_t}^{(j)},\qquad x_t=x_1,x_2, \tag{9}$$

$$\begin{aligned}\varsigma_{1,x,,x_t}^{(j)}=&T_{n-|x_t-x|+2}^{(j)}+(h_1+h_2-2)(T_{n-|x_t-x|+1}^{(j)}-T_{n-|x_t-x|-1}^{(j)})\\ &+(h_1h_2-h_1-h_2)T_{n-|x_t-x|}^{(j)}-(h_1-1)(h_2-1)T_{n-|x_t-x|-2}^{(j)},\end{aligned}$$

$$\begin{aligned}\varsigma_{2,x,x_t}^{(j)}=&(h_2-h_1)T_{n-x_t-x}^{(j)}+(h_1-1)T_{n-x_t-x+2}^{(j)}\\ &-(h_2-1)T_{n-x_t-x-2}^{(j)}+(h_1-1)(h_2-1)(T_{n-x_t-x+1}^{(j)}-T_{n-x_t-x-1}^{(j)}),\end{aligned}$$

$$h=\frac{r}{r_0},\quad h_1=\frac{r_1}{r_0},\quad h_2=\frac{r_2}{r_0}, \tag{10}$$

$$P_{k,j}=\sin\frac{k(2j-1)\pi}{2m+1},\quad k=y,y_1,y_2, \tag{11}$$

$$H_n^{(j)}=T_{n+1}^{(j)}+(h_1+h_2-2)T_n^{(j)}+(h_1-1)(h_2-1)T_{n-1}^{(j)}, \tag{12}$$

$$\begin{aligned}T_k^{(j)}&=T_k^{(j)}(\cosh\sigma_j)=\frac{\sinh(k\sigma_j)}{\sinh\sigma_j},\\ \cosh\sigma_j&=\frac{\varpi_j}{2},\quad \sigma\in\mathbf{R},\end{aligned} \tag{13}$$

and

$$\varpi_j = 2 + 2\frac{r}{r_0} - 2\frac{r}{r_0}\cos\frac{(2j-1)\pi}{2m+1}, \qquad (14)$$

for $k = n-|x_1-x|+2$, $n-|x_1-x|+1$, $n-|x_1-x|$, $n-|x_1-x|-1$, $n-|x_1-x|-2$, $n-x_1-x+2$, $n-x_1-x+1$, $n-x_1-x$, $n-x_1-x-1$, $n-x_1-x-2$, $n-|x_2-x|+2$, $n-|x_2-x|+1$, $n-|x_2-x|$, $n-|x_2-x|-1$, $n-|x_2-x|-2$, $n-x_2-x+2$, $n-x_2-x+1$, $n-x_2-x$, $n-x_2-x-1$, $n-x_2-x-2$, $n+1$, n, $n-1$, 0.5, and $\langle \Upsilon_{x,x_t}, P_k\rangle$, $\langle P_y, T_{0.5}\rangle$ and $\langle \alpha, H_n\rangle$ are inner products. The APF (8) can solve the potential of any node concerning the origin, satisfying $0 \leqslant x \leqslant n$, $1 \leqslant y \leqslant m$.

The APF (8) not only replaces the piecewise function of APF (1) with a single absolute value function, but also replaces the original exponential operation with the CPs of the second kind, and adopts expressed in inner product form. Compared to the APF (1), the APF (8) exhibits higher computational performance and scalability. Additionally, the APF (8) is another expression derived from refining Tan's APF (1).

Assuming that the voltage at the origin, O, is zero, i.e., $V_0^{(0)} = 0$, the potential at any node concerning the origin can be expressed using Ohm's law:

$$\frac{U_{m\times n}(x,y)}{J} = \frac{V_x^{(y)} - V_0^{(0)}}{J}, \qquad (15)$$

where $V_x^{(y)}$ is the node voltage.

THE DETAILED PROCESS OF OBTAINING THE ANALYTICAL POTENTIAL FUNCTION

In this section, we employ the discrete sine transform of the sixth type (DST-VI) to perform orthogonal diagonalization on the tridiagonal quasi-Toeplitz matrix. Additionally, we introduce the CPs of the second class to represent the Horadam sequences. Furthermore, we enhance the original piecewise functions by formulating them as a single analytical function incorporating absolute values.

The Horadam sequence [25] is defined as follows:

$$\mathscr{W}_k = p\mathscr{W}_{k-1} - q\mathscr{W}_{k-2}, \quad \mathscr{W}_0 = a, \quad \mathscr{W}_1 = b, \qquad (16)$$

where $k \in \mathbb{N}_0^+$, $k \geqslant 2$, $a, b, p, q \in \mathbb{C}$, $\mathbb{N}_0^+$ is set of nonnegative integers and $\mathbb{C}$ is the all complex numbers.

The Horadam sequences [25] are represented by the CPs of the second class, and the exact function of $\mathscr{W}_k$ is given by

$$\mathscr{W}_k = q^{\frac{k}{2}}\left[\frac{b}{\sqrt{q}}\mathscr{U}_{k-1}\left(\frac{p}{2\sqrt{q}}\right) - a\mathscr{U}_{k-2}\left(\frac{p}{2\sqrt{q}}\right)\right], \qquad (17)$$

where

$$\begin{aligned} \mathscr{U}_k &= \mathscr{U}_k(\cos\sigma) = \frac{\sin(k+1)\sigma}{\sin\sigma}, \\ \cos\sigma &= \frac{p}{2\sqrt{q}}, \qquad \sigma \in \mathbb{C}, \end{aligned} \qquad (18)$$

is the CP of the second class [24]. According to the physical interpretation of this study, Eq. (18) should be expressed as follows:

$$\begin{aligned} \mathscr{U}_k &= \mathscr{U}_k(\cosh\sigma) = \frac{\sinh(k+1)\sigma}{\sinh\sigma}, \\ \cosh\sigma &= \frac{p}{2\sqrt{q}}, \qquad \sigma \in \mathbb{R}, \end{aligned} \qquad (19)$$

where $\mathbb{R}$ is the set of real number.

First, the derivation of Eq. (2) represented by the CPs of the second class is given.

Remark 1 Based on Eqs. (2), (7), (16), (17), and (19), the process of obtaining the APF (8) through the improvement of the APF (1) with the CP of the second class can be explained. Referring to Eq. (7), we have $\lambda_j + \bar{\lambda}_j = \varpi_j$ and $\lambda_j \cdot \bar{\lambda}_j = 1$. Substituting these equations into Eq. (16), we find that $F_k^{(j)}$ satisfies the three-term recurrence relation:

$$F_k^{(j)} = \varpi_j F_{k-1}^{(j)} - F_{k-2}^{(j)}, \quad F_0^{(j)} = 0, \quad F_1^{(j)} = 1, \qquad (20)$$

where $p = \varpi_j$, $q = 1$, $F_k^{(j)}$ and ϖ_j are given by Eqs. (2) and (7), respectively. By Eqs. (2), (16), (17), and (19), the expression for $F_k^{(j)}$ can be obtained:

$$F_k^{(j)} = \frac{\lambda_j^k - \bar{\lambda}_j^k}{\lambda_j - \bar{\lambda}_j} = \mathscr{U}_{k-1}^{(j)}(\cosh\sigma_j) = T_k^{(j)}(\cosh\sigma_j). \qquad (21)$$

For ease of expression, let

$$\begin{aligned} \mathscr{U}_{k-1}^{(j)}(\cosh\sigma_j) = T_k^{(j)}(\cosh\sigma_j) &= \frac{\sinh(k\sigma_j)}{\sinh\sigma_j}, \\ \cosh\sigma_j &= \frac{\varpi_j}{2}, \qquad \sigma_j \in \mathbb{R}. \end{aligned} \qquad (22)$$

Following this, we convert the piecewise function (4) into a function (9) that incorporates absolute values.

Remark 2 The piecewise function (4) is expanded as follows:

$$\begin{aligned} \beta_{x_s,x}^{(i)} &= \begin{cases} \alpha_{1,x_s}^{(i)}\alpha_{2,n-x}^{(i)}, & \text{if } x \geqslant x_s, \\ \alpha_{1,x}^{(i)}\alpha_{2,n-x_s}^{(i)}, & \text{if } x \leqslant x_s, \end{cases} \\ &= \begin{cases} \Delta F_{x_s}^{(i)}\Delta F_{n-x}^{(i)} + (b_1-1)\Delta F_{x_s-1}^{(i)}\Delta F_{n-x}^{(i)} \\ \quad +(b_2-1)\Delta F_{x_s}^{(i)}\Delta F_{n-x-1}^{(i)} \\ \quad +(b_1-1)(b_2-1)\Delta F_{x_s-1}^{(i)}\Delta F_{n-x-1}^{(i)}, & \text{if } x \geqslant x_s, \\ \Delta F_{x}^{(i)}\Delta F_{n-x_s}^{(i)} + (b_1-1)\Delta F_{x-1}^{(i)}\Delta F_{n-x_s}^{(i)} \\ \quad +(b_2-1)\Delta F_{x}^{(i)}\Delta F_{n-x_s-1}^{(i)} \\ \quad +(b_1-1)(b_2-1)\Delta F_{x-1}^{(i)}\Delta F_{n-x_s-1}^{(i)}, & \text{if } x \leqslant x_s, \end{cases} \end{aligned} \qquad (23)$$

where $\alpha_{s,x}^{(i)}=\Delta F_x^{(i)}+(b_s-1)\Delta F_{x-1}^{(i)}$, $\Delta F_k^{(i)}=F_{k+1}^{(i)}-F_k^{(i)}$, $F_k^{(i)}=\frac{(\lambda_j^k-\bar{\lambda}_j^k)}{(\lambda_j-\bar{\lambda}_j)}$, $b_s=r_s/r_0$.

The piecewise function (23) is decomposed for computation as follows. When $x\geqslant x_s$, $s=1,2$,

$$\begin{aligned}
\Delta F_{x_s}^{(i)}\Delta F_{n-x}^{(i)} &= (F_{x_s+1}^{(i)}-F_{x_s}^{(i)})(F_{n-x+1}^{(i)}-F_{n-x}^{(i)})\\
&=\Bigg(\frac{\lambda_i^{n-x+x_s+2}+\bar{\lambda}_i^{n-x+x_s+2}-\lambda_i^{n-x+x_s+1}-\bar{\lambda}_i^{n-x+x_s+1}}{(\lambda_i-\bar{\lambda}_i)^2}\\
&\quad-\frac{\lambda_i^{n-x+x_s+1}+\bar{\lambda}_i^{n-x+x_s+1}-\lambda_i^{n-x+x_s}-\bar{\lambda}_i^{n-x+x_s}}{(\lambda_i-\bar{\lambda}_i)^2}\Bigg)\\
&\quad+\Bigg(\frac{\lambda_i^{n-x-x_s+1}+\bar{\lambda}_i^{n-x-x_s+1}-\lambda_i^{n-x-x_s}-\bar{\lambda}_i^{n-x-x_s}}{(\lambda_i-\bar{\lambda}_i)^2}\\
&\quad-\frac{\lambda_i^{n-x-x_s}+\bar{\lambda}_i^{n-x-x_s}-\lambda_i^{n-x-x_s-1}-\bar{\lambda}_i^{n-x-x_s-1}}{(\lambda_i-\bar{\lambda}_i)^2}\Bigg)\\
&=\frac{(\lambda_i+\bar{\lambda}_i-2)(\lambda_i^{n-x+x_s+1}+\bar{\lambda}_i^{n-x+x_s+1}+\lambda_i^{n-x-x_s}+\bar{\lambda}_i^{n-x-x_s})}{(\lambda_i-\bar{\lambda}_i)^2}\\
&=\frac{(\lambda_i^{0.5}-\bar{\lambda}_i^{0.5})^2}{(\lambda_i-\bar{\lambda}_i)^2}\left(\lambda_i^{n-x+x_s+1}+\bar{\lambda}_i^{n-x+x_s+1}+\lambda_i^{n-x-x_s}+\bar{\lambda}_i^{n-x-x_s}\right)\\
&=(F_{0.5}^{(i)})^2\left(F_{n-(x-x_s)+2}^{(i)}-F_{n-(x-x_s)}^{(i)}+F_{n-x-x_s+1}^{(i)}-F_{n-x-x_s-1}^{(i)}\right). \qquad (24)
\end{aligned}$$

When $x\leqslant x_s$, $s=1,2$,

$$\begin{aligned}
\Delta F_x^{(i)}\Delta F_{n-x_s}^{(i)} &= (F_{x+1}^{(i)}-F_x^{(i)})(F_{n-x_s+1}^{(i)}-F_{n-x_s}^{(i)})\\
&=\Bigg(\frac{\lambda_i^{n-x_s+x+2}+\bar{\lambda}_i^{n-x_s+x+2}-\lambda_i^{n-x_s+x+1}-\bar{\lambda}_i^{n-x_s+x+1}}{(\lambda_i-\bar{\lambda}_i)^2}\\
&\quad-\frac{\lambda_i^{n-x_s+x+1}+\bar{\lambda}_i^{n-x_s+x+1}-\lambda_i^{n-x_s+x}-\bar{\lambda}_i^{n-x_s+x}}{(\lambda_i-\bar{\lambda}_i)^2}\Bigg)\\
&\quad+\Bigg(\frac{\lambda_i^{n-x_s-x+1}+\bar{\lambda}_i^{n-x_s-x+1}-\lambda_i^{n-x_s-x}-\bar{\lambda}_i^{n-x_s-x}}{(\lambda_i-\bar{\lambda}_i)^2}\\
&\quad-\frac{\lambda_i^{n-x_s-x}+\bar{\lambda}_i^{n-x_s-x}-\lambda_i^{n-x_s-x-1}-\bar{\lambda}_i^{n-x_s-x-1}}{(\lambda_i-\bar{\lambda}_i)^2}\Bigg)\\
&=\frac{(\lambda_i+\bar{\lambda}_i-2)(\lambda_i^{n-x_s+x+1}+\bar{\lambda}_i^{n-x_s+x+1}+\lambda_i^{n-x_s-x}+\bar{\lambda}_i^{n-x_s-x})}{(\lambda_i-\bar{\lambda}_i)^2}\\
&=\frac{(\lambda_i^{0.5}-\bar{\lambda}_i^{0.5})^2}{(\lambda_i-\bar{\lambda}_i)^2}(\lambda_i^{n-x_s+x+1}+\bar{\lambda}_i^{n-x_s+x+1}+\lambda_i^{n-x_s-x}+\bar{\lambda}_i^{n-x_s-x})\\
&=(F_{0.5}^{(i)})^2\left(F_{n-(x_s-x)+2}^{(i)}-F_{n-(x_s-x)}^{(i)}+F_{n-x_s-x+1}^{(i)}-F_{n-x_s-x-1}^{(i)}\right). \qquad (25)
\end{aligned}$$

Based on Eqs. (24) and (25), a portion of the piecewise function can be transformed into a function involving absolute value, as presented below:

$$\left.\begin{matrix}\Delta F_{x_s}^{(i)}\Delta F_{n-x}^{(i)},\ \text{if } x\geqslant x_s\\ \Delta F_x^{(i)}\Delta F_{n-x_s}^{(i)},\ \text{if } x\leqslant x_s\end{matrix}\right\}=(F_{0.5}^{(i)})^2\Big(F_{n-|x_s-x|+2}^{(i)}-F_{n-|x_s-x|}^{(i)}+F_{n-x_s-x+1}^{(i)}-F_{n-x_s-x-1}^{(i)}\Big),\quad s=1,2. \qquad (26)$$

Based on the methodology outlined above, the remaining segments of the piecewise function are respectively represented as follows:

$$\left.\begin{matrix}(b_1-1)\Delta F_{x_s-1}^{(i)}\Delta F_{n-x}^{(i)},\ \text{if } x\geqslant x_s\\ (b_1-1)\Delta F_{x-1}^{(i)}\Delta F_{n-x_s}^{(i)},\ \text{if } x\leqslant x_s\end{matrix}\right\}=(b_1-1)(F_{0.5}^{(i)})^2\Big(F_{n-|x_s-x|+1}^{(i)}-F_{n-|x_s-x|-1}^{(i)}+F_{n-x_s-x+2}^{(i)}-F_{n-x_s-x}^{(i)}\Big),\quad s=1,2, \qquad (27)$$

$$\left.\begin{matrix}(b_2-1)\Delta F_{x_s}^{(i)}\Delta F_{n-x-1}^{(i)},\ \text{if } x\geqslant x_s\\ (b_2-1)\Delta F_x^{(i)}\Delta F_{n-x_s-1}^{(i)},\ \text{if } x\leqslant x_s\end{matrix}\right\}=(b_2-1)(F_{0.5}^{(i)})^2\Big(F_{n-|x_s-x|+1}^{(i)}-F_{n-|x_s-x|-1}^{(i)}+F_{n-x_s-x}^{(i)}-F_{n-x_s-x-2}^{(i)}\Big),\quad s=1,2, \qquad (28)$$

$$\begin{aligned}
&\left.\begin{matrix}(b_1-1)(b_2-1)\Delta F_{x_s-1}^{(i)}\Delta F_{n-x-1}^{(i)},\ \text{if } x\geqslant x_s\\ (b_1-1)(b_2-1)\Delta F_{x-1}^{(i)}\Delta F_{n-x_s-1}^{(i)},\ \text{if } x\leqslant x_s\end{matrix}\right\}\\
&\quad=(b_1-1)(b_2-1)(F_{0.5}^{(i)})^2\Big(F_{n-|x_s-x|}^{(i)}-F_{n-|x_s-x|-2}^{(i)}+F_{n-x_s-x+1}^{(i)}-F_{n-x_s-x-1}^{(i)}\Big),\quad s=1,2. \qquad (29)
\end{aligned}$$

We replace each part of the piecewise function (23) by functions (26), (27), (28) and (29) containing absolute values, respectively, and then arrange them according to the combination of function (23), the piecewise function (23) is completely rewritten as a single function involving absolute values, given as follows:

$$\beta_{x_s,x}^{(i)}=(F_{0.5}^{(i)})^2(\varsigma_{1,x,x_s}^{(i)}+\varsigma_{2,x,x_s}^{(i)}),\qquad s=1,2, \qquad (30)$$

where

$$\begin{aligned}
\varsigma_{1,x,x_s}^{(i)} &= F_{n-|x_s-x|+2}^{(i)}+(b_1+b_2-2)\Big(F_{n-|x_s-x|+1}^{(i)}-F_{n-|x_s-x|-1}^{(i)}\Big)\\
&\quad+(b_1b_2-b_1-b_2)F_{n-|x_s-x|}^{(i)}-(b_1-1)(b_2-1)F_{n-|x_s-x|-2}^{(i)},\\
\varsigma_{2,x,x_s}^{(i)} &= (b_2-b_1)F_{n-x_s-x}^{(i)}+(b_1-1)F_{n-x_s-x+2}^{(i)}-(b_2-1)F_{n-x_s-x-2}^{(i)}\\
&\quad+(b_1-1)(b_2-1)(F_{n-x_s-x+1}^{(i)}-F_{n-x_s-x-1}^{(i)}).
\end{aligned}$$

Based on Eq. (21) and function (30), the piecewise function (4) is transformed into a single function (9) containing absolute values.

In summary, we derive the APF (8).

To achieve efficient potential computation, it is essential to carry out orthogonal diagonalization of the matrix $\mathbf{B}_m$. This process aims to find a set of orthogonal eigenvectors and corresponding eigenvalues that allow for faster calculations.

$$\mathbf{B}_m=\begin{pmatrix}2+2h & -h & 0 & \cdots & \cdots & 0\\ -h & 2+2h & -h & \ddots & & \vdots\\ 0 & -h & \ddots & \ddots & \ddots & \vdots\\ \vdots & \ddots & \ddots & \ddots & -h & 0\\ \vdots & & \ddots & -h & 2+2h & -h\\ 0 & \cdots & \cdots & 0 & -h & 2+h\end{pmatrix}_{m\times m}, \qquad (31)$$

where $h = r/r_0$.

The eigenvalues of $\mathbf{B}_m$ are

$$\varpi_j = 2 + 2h - 2h\cos\tfrac{(2j-1)\pi}{2m+1}, \quad j = 1, 2, \ldots, m, \quad (32)$$

and the corresponding eigenvector $\alpha^{(j)} = (\alpha_1^{(j)}, \ldots, \alpha_m^{(j)})^{\mathrm{T}}$ where

$$\alpha_k^{(j)} = \tfrac{2}{\sqrt{2m+1}} \sin\tfrac{(2j-1)k\pi}{2m+1}, \quad j, k = 1, 2, \ldots, m. \quad (33)$$

Based on Eq. (33), the orthogonal matrix $\mathbb{S}_m^{\mathrm{VI}}$ can be obtained as follows:

$$\mathbb{S}_m^{\mathrm{VI}} = \tfrac{2}{\sqrt{2m+1}} \left(\sin\tfrac{(2j-1)k\pi}{2m+1}\right)_{j,k=1}^{m}. \quad (34)$$

As it is well known, the matrix $\mathbb{S}_m^{\mathrm{VI}}$ is famous for being the discrete sine transform of the sixth kind (DST-VI) [26–28]. The inverse and transpose matrices of $\mathbb{S}_m^{\mathrm{VI}}$ are provided below:

$$(\mathbb{S}_m^{\mathrm{VI}})^{-1} = (\mathbb{S}_m^{\mathrm{VI}})^{\mathrm{T}} = (\mathbb{S}_m^{\mathrm{VII}}). \quad (35)$$

The matrix $\mathbf{B}_m$ can be orthogonally diagonalized as follows:

$$(\mathbb{S}_m^{\mathrm{VI}})^{-1}\mathbf{B}_m(\mathbb{S}_m^{\mathrm{VI}}) = \mathrm{diag}(\varpi_1, \varpi_2, \ldots, \varpi_m), \quad (36)$$

i.e.,

$$(\mathbb{S}_m^{\mathrm{VI}})^{-1}\mathbf{B}_m = \mathrm{diag}(\varpi_1, \varpi_2, \ldots, \varpi_m)(\mathbb{S}_m^{\mathrm{VI}})^{-1}, \quad (37)$$

where ϖ_j, $(j = 1, 2, \ldots, m)$ is given by Eq. (32). In conclusion, Eqs. (32) and (33) are the eigenvalues and eigenvectors of matrix $\mathbf{B}_m$ respectively.

Based on Kirchhoff's laws, Tan [23] conducted a study on resistor networks and derived the matrix equation for the resistor network as follows:

$$\mathbf{V}_{k+1} = \mathbf{B}_m\mathbf{V}_k - \mathbf{V}_{k-1} - r\mathbf{I}_y\tau_{x,k}, \quad (38)$$

where

$$\mathbf{V}_k = [V_k^{(1)}, V_k^{(2)}, \ldots V_k^{(m)}]^{\mathrm{T}} \qquad (0 \leqslant k \leqslant n), \quad (39)$$

$$I_y^{(j)} = J(\tau_{y_1,j} - \tau_{y_2,j}), \quad (40)$$

$\mathbf{B}_m$ is given by Eq. (31), $\tau_{x,k}$ and $\tau_{y,j}$ are defined by $\tau_{x,k}(x = k) = 1$, $\tau_{x,k}(x \neq k) = 0$ and $\tau_{y,j}(y = j) = 1$, $\tau_{y,j}(y \neq j) = 0$, respectively.

Remark 3 Let

$$(\mathbb{S}_m^{\mathrm{VI}})^{-1}\mathbf{V}_k = \mathbf{L}_k \quad (41)$$

where

$$\mathbf{L}_k = [L_k^{(1)}, L_k^{(2)}, \ldots, L_k^{(m)}]^{\mathrm{T}} \qquad (0 \leqslant k \leqslant n). \quad (42)$$

We have

$$\mathbf{V}_k = \mathbb{S}_m^{\mathrm{VI}}\mathbf{L}_k. \quad (43)$$

Tan [23] proposed an analytical function for the arbitrary nodal voltage of the $m \times n$ fan resistor network, as follows:

$$V_k^{(y)} = J\frac{4r}{2m+1}\sum_{i=1}^{m}\frac{\beta_{x,x_1}^{(i)}\zeta_{1,i} + \beta_{x,x_2}^{(i)}\zeta_{2,i}}{(t_i - 2)G_n^{(i)}}\sin(y\theta_i), \quad (44)$$

where $t_i = 2(1+b) - 2b\cos\theta_i$, $b = r/r_0$, $\zeta_{1,i} = \sin y_1\theta_i$, $\zeta_{2,i} = -\sin y_2\theta_i$, $\beta_{x,x_k}^{(i)}$, $G_n^{(i)}$ and θ_i are given by Eqs. (4), (5) and (6), respectively.

Based on Eq. (21) and function (30), the piecewise function (44) is reexpressed as a single function, solely consisting of absolute values, represented by the CPs of the second class.

$$V_x^{(y)} = J\frac{4r}{2m+1}\sum_{j=1}^{m}\frac{\Upsilon_{x,x_1}^{(j)}P_{y_1,j} - \Upsilon_{x,x_2}^{(j)}P_{y_2,j}}{(\varpi_j - 2)H_n^{(j)}}P_{y,j}(T_{0.5}^{(j)})^2, \quad (45)$$

where $\Upsilon_{x,x_k}^{(j)}$, $P_{k,j}$, ϖ_j, $H_n^{(j)}$ and $T_k^{(j)}$ are defined by Eqs. (9), (11), (14), (12) and (13), respectively.

Based on Eqs. (34), (35), (41) and (45), $L_x^{(j)}$ can be expressed as follows:

$$L_x^{(j)} = \frac{2rJ}{\sqrt{2m+1}}\frac{\Upsilon_{x,x_1}^{(j)}P_{y_1,j} - \Upsilon_{x,x_2}^{(j)}P_{y_2,j}}{(\varpi_j - 2)H_n^{(j)}}(T_{0.5}^{(j)})^2 \quad (46)$$

for $0 \leqslant x \leqslant n$, where $\Upsilon_{x,x_t}^{(j)}$, $P_{k,j}$, ϖ_j, $H_n^{(j)}$ and $T_k^{(j)}$ are given by Eqs. (9), (11), (14), (12) and (13), respectively.

ANALYTICAL FUNCTIONS OF POTENTIAL IN SPECIAL CASES AND 3D POTENTIAL DISTRIBUTION MAPS

The APF (8) represents the overall APF of the fan resistor network, which, although meaningful, can be rather complex to comprehend. Therefore, we provide several specific cases of the APF (8) to comprehend its meaning. Furthermore, based on the specific APFs, we employ 3D views to show the potential of each node. And we can visually illustrate the influence for the position of current J, h, h_1, and h_2 on the potential distribution.

The cases where the current J is input and output at a specific position

Based on the APF (8), and assuming uniform resistor values of $r = r_0 = r_1 = r_2 = 1$ (i.e., $h = h_1 = h_2 = 1$), we can obtain the APFs for the current J at the specific input point $d_1(x_1, y_1)$ or output point $d_2(x_2, y_2)$.

Special 1. When the current J is input at any point and output at the origin $O(0, 0)$, the analytical function of the potential is given by:

$$\frac{U_{m\times n}(x,y)}{J} = \frac{2r_0}{2m+1}\sum_{j=1}^{m}\frac{P_{y_1,j}P_{y,j}}{(1-\cos\frac{(2j-1)\pi}{2m+1})T_{n+1}^{(j)}}\Upsilon_{x,x_1}^{(j)}(T_{0.5}^{(j)})^2, \quad (47)$$

where

$$\Upsilon^{(j)}_{x,x_1} = T^{(j)}_{n-|x_1-x|+2} - T^{(j)}_{n-|x_1-x|} + T^{(j)}_{n-x_1-x+1} - T^{(j)}_{n-x_1-x-1}, \quad (48)$$

$P_{k,j}$ and $T^{(j)}_k$ are provided by Eqs. (11) and (13), respectively.

When $m = n = 80$, $x_1 = y_1 = 40$, and $x_2 = y_2 = 0$, the APF (47) is expressed as:

$$\frac{U_{80\times 80}(x,y)}{J} = \frac{2}{161}\sum_{j=1}^{80} \frac{\sin(\frac{40(2j-1)\pi}{161})\sin(\frac{y(2j-1)\pi}{161})}{(1-\cos\frac{(2j-1)\pi}{161})T^{(j)}_{81}} \Upsilon^{(j)}_{x,40}(T^{(j)}_{0.5})^2, \quad (49)$$

where

$$\Upsilon^{(j)}_{x,40} = T^{(j)}_{82-|40-x|} - T^{(j)}_{80-|40-x|} + T^{(j)}_{41-x} - T^{(j)}_{39-x}, \quad (50)$$

and

$$T^{(j)}_k = T^{(j)}_k(\cosh\sigma_j) = \frac{\sinh(k\sigma_j)}{\sinh\sigma_j}, \qquad \cosh\sigma_j = \frac{\varpi_j}{2} = 2-\cos\frac{(2j-1)\pi}{161}, \quad (51)$$

$k = 82-|40-x|, 80-|40-x|, 41-x, 39-x, 81, 0.5$.

A three-dimensional view of the potential is generated using Matlab, as depicted in Fig. 2.

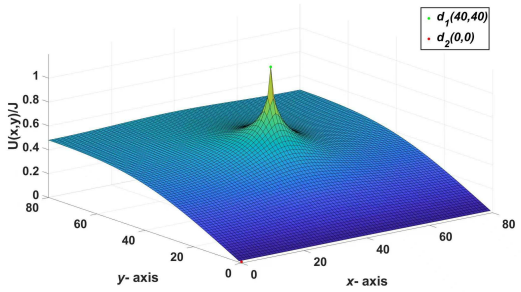

Fig. 2: A 3D view for generating procedure of the $U_{80\times 80}(x,y)/J$ map in Eq. (47).

Special 2. Given that the current J flows in and out along the same longitude, i.e., $x_1 = x_2$ for the input point $d_1(x_1, y_1)$ and the output point $d_2(x_2, y_2)$, the analytical function of the potential is expressed as follows:

$$\frac{U_{m\times n}(x,y)}{J} = \frac{2r_0}{2m+1}\sum_{j=1}^{m} \frac{(P_{y_1,j}-P_{y_2,j})\Upsilon^{(j)}_{x,x_1}}{(1-\cos\frac{(2j-1)\pi}{2m+1})T^{(j)}_{n+1}} P_{y,j}(T^{(j)}_{0.5})^2, \quad (52)$$

where $P_{k,j}$, $T^{(j)}_k$ and $\Upsilon^{(j)}_{x,x_1}$ are defined in Eqs. (11), (13) and (48), respectively.

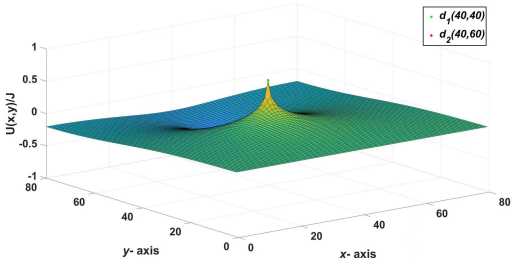

Fig. 3: A 3D view for generating procedure of the $U_{80\times 80}(x,y)/J$ map in Eq. (52).

Consider $m = n = 80$, $x_1 = x_2 = y_1 = 40$, and $y_2 = 60$. The potential distribution described by Eq. (52) is depicted in Fig. 3.

Special 3. When the current J flows from the input point $d_1(x_1, y_1)$ to the output point $d_2(x_2, y_2)$, where $y_1 = y_2$, the analytical function of the potential is expressed as follows:

$$\frac{U_{m\times n}(x,y)}{J} = \frac{2r_0}{2m+1}\sum_{j=1}^{m} \frac{(\Upsilon^{(j)}_{x,x_1}-\Upsilon^{(j)}_{x,x_2})P_{y_1,j}P_{y,j}}{(1-\cos\frac{(2j-1)\pi}{2m+1})T^{(j)}_{n+1}} (T^{(j)}_{0.5})^2, \quad (53)$$

where

$$\Upsilon^{(j)}_{x,x_2} = T^{(j)}_{n-|x_2-x|+2} - T^{(j)}_{n-|x_2-x|} + T^{(j)}_{n-x_2-x+1} - T^{(j)}_{n-x_2-x-1}, \quad (54)$$

$P_{k,j}$, $T^{(j)}_k$ and $\Upsilon^{(j)}_{x,x_1}$ are given by Eqs. (11), (13) and (48), respectively.

Based on the APF (53), when $m = n = 80$, we consider the specific values $x_1 = y_1 = y_2 = 40$ and $x_2 = 60$. The potential distribution in Eq. (53) is illustrated in Fig. 4.

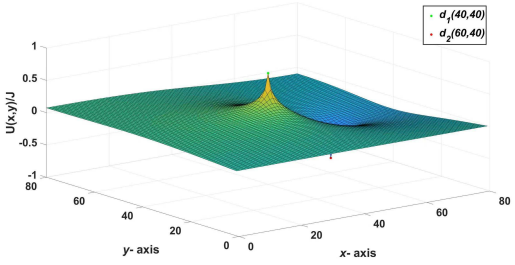

Fig. 4: A 3D view for generating procedure of the $U_{80\times 80}(x,y)/J$ map in Eq. (53).

The cases where h, h_1 and h_2 are specific values

The current J has fixed input positions $d_1(x_1, y_1)$ and output positions $d_2(x_2, y_2)$, where $x_1 = y_1 = 40$ and $x_2 = y_2 = 60$. The APFs are studied for specific values

of h, h_1, and h_2, respectively.

Special 1. Assuming the $h_1 = h_2 = 1$ and $h = 0.1$, the analytical function of potential is:

$$\frac{U_{m\times n}(x,y)}{J} = \frac{4r}{2m+1}\sum_{j=1}^{m}\frac{\Upsilon^{(j)}_{x,x_1}P_{y_1,j}-\Upsilon^{(j)}_{x,x_2}P_{y_2,j}}{(\varpi_j-2)T^{(j)}_{n+1}}P_{y,j}(T^{(j)}_{0.5})^2, \quad (55)$$

where

$$\varpi_j = \frac{11}{5}-\frac{1}{5}\cos\frac{(2j-1)\pi}{2m+1}, \quad (56)$$

$P_{k,j}$, $T^{(j)}_k$, $\Upsilon^{(j)}_{x,x_1}$ and $\Upsilon^{(j)}_{x,x_2}$ are given by Eqs. (11), (13), (48) and (54), respectively.

When $m = n = 80$, $r_0 = r_1 = r_2 = 10$, and $r = 1$, the APF (55) can be expressed as follows:

$$\frac{U_{80\times 80}(x,y)}{J} = \frac{4}{161}\sum_{j=1}^{80}\frac{\sin(\frac{40(2j-1)\pi}{161})\Upsilon^{(j)}_{x,40}-\sin(\frac{60(2j-1)\pi}{161})\Upsilon^{(j)}_{x,60}}{(\varpi_j-2)T^{(j)}_{81}} \times \sin\Big(\frac{y(2j-1)\pi}{161}\Big)(T^{(j)}_{0.5})^2, \quad (57)$$

where

$$\varpi_j = \frac{11}{5}-\frac{1}{5}\cos\frac{(2j-1)\pi}{161}, \quad (58)$$

$$T^{(j)}_k = T^{(j)}_k\big(\cosh\sigma_j\big) = \frac{\sinh(k\sigma_j)}{\sinh\sigma_j}, \quad \cosh\sigma_j = \frac{11}{10}-\frac{1}{10}\cos\frac{(2j-1)\pi}{161},\ k = 81, 0.5, \quad (59)$$

$$\Upsilon^{(j)}_{x,60} = T^{(j)}_{82-|60-x|}-T^{(j)}_{80-|60-x|}+T^{(j)}_{21-x}-T^{(j)}_{19-x}, \quad (60)$$

and $\Upsilon^{(j)}_{x,40}$ is given by Eq. (50). The potential distribution in Eq. (57) is shown in Fig. 5.

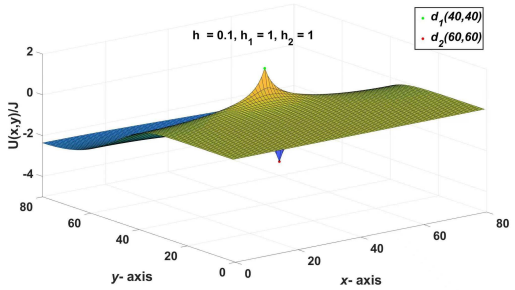

Fig. 5: A 3D view for generating procedure of the $U_{80\times 80}(x,y)/J$ map in Eq. (57).

Special 2. In the case where $h_1 = h_2 = 1$ and $h = 0.01$, the analytical function for the potential is expressed as follows:

$$\frac{U_{m\times n}(x,y)}{J} = \frac{4r}{2m+1}\sum_{j=1}^{m}\frac{\Upsilon^{(j)}_{x,x_1}P_{y_1,j}-\Upsilon^{(j)}_{x,x_2}P_{y_2,j}}{(\varpi_j-2)T^{(j)}_{n+1}}P_{y,j}(T^{(j)}_{0.5})^2, \quad (61)$$

where

$$\varpi_j = \frac{101}{50}-\frac{1}{50}\cos\frac{(2j-1)\pi}{2m+1}, \quad (62)$$

and $P_{k,j}$, $T^{(j)}_k$ and $\Upsilon^{(j)}_{x,x_1}$ and $\Upsilon^{(j)}_{x,x_2}$ are defined by Eqs. (11), (13), (48) and (54), respectively.

In the APF (61), we set $m = n = 80$, $r_0 = r_1 = r_2 = 100$, and $r = 1$. The potential distribution plot, generated using Matlab, is illustrated in Fig. 6.

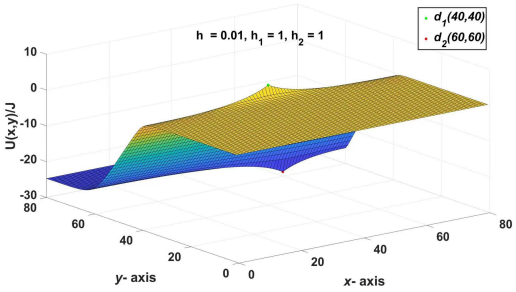

Fig. 6: A 3D view for generating procedure of the $U_{80\times 80}(x,y)/J$ map in Eq. (61).

Special 3. In the $m \times n$ fan resistor network, where $h = 1$, $h_1 = 0.1$, and $h_2 = 0.01$, the analytic expression for the potential is given by

$$\frac{U_{m\times n}(x,y)}{J} = \frac{4r}{2m+1}\sum_{j=1}^{m}\frac{\Upsilon^{(j)}_{x,x_1}P_{y_1,j}-\Upsilon^{(j)}_{x,x_2}P_{y_2,j}}{(\varpi_j-2)H^{(j)}_n}P_{y,j}(T^{(j)}_{0.5})^2, \quad (63)$$

where

$$\Upsilon^{(j)}_{x,x_t} = \varsigma^{(j)}_{1,x,,x_t}+\varsigma^{(j)}_{2,x,,x_t}, \qquad x_t = x_1, x_2, \quad (64)$$

$$\varsigma^{(j)}_{1,x,,x_t} = T^{(j)}_{n-|x_t-x|+2}+0.89(T^{(j)}_{n-|x_t-x|+1}-T^{(j)}_{n-|x_t-x|-1}) -0.109T^{(j)}_{n-|x_t-x|}-0.891T^{(j)}_{n-|x_t-x|-2},$$

$$\varsigma^{(j)}_{2,x,x_t} = -0.09T^{(j)}_{n-x_t-x}-0.9T^{(j)}_{n-x_t-x+2}+0.99T^{(j)}_{n-x_t-x-2} +0.891(T^{(j)}_{n-x_t-x+1}-T^{(j)}_{n-x_t-x-1}),$$

$$\varpi_j = 4-2\cos(\frac{(2j-1)\pi}{2m+1}), \quad (65)$$

$$H^{(j)}_n = T^{(j)}_{n+1}-1.89T^{(j)}_n+0.891T^{(j)}_{n-1}, \quad (66)$$

$P_{k,j}$ and $T_k^{(j)}$ can be given by Eqs. (11) and (13), respectively.

When $m = n = 80$, $r = r_0 = 1$, $r_1 = 10$, and $r_2 = 100$. The potential distribution described by Eq. (63) is illustrated in Fig. 7.

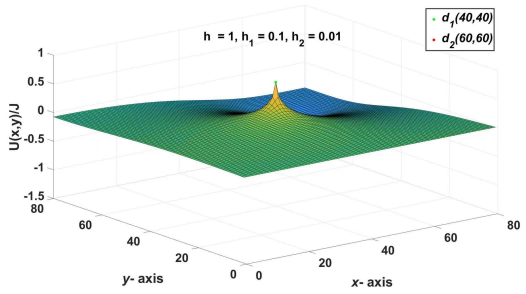

Fig. 7: A 3D view for generating procedure of the $U_{80\times80}(x,y)/J$ map in Eq. 63).

A FAST ALGORITHM FOR COMPUTING POTENTIAL

In this section, we implement a fast algorithm for calculating the potential. The algorithm is based on DST-VI and Eqs. (14), (13), (15), (38), (43), and (46).

The fast algorithm follows the following overall idea: Firstly, we obtain the initial values $\mathbf{L}_0$ and $\mathbf{L}_1$ using Eq. (46). Secondly, we solve for $\mathbf{V}_0$ and $\mathbf{V}_1$ respectively, as described in Eq. (43). Finally, we design a fast matrix-vector multiplication algorithm, i.e., Algorithm 1. By applying $\mathbf{V}_0$, $\mathbf{V}_1$, Algorithm 1, and Eq. (38), we recursively obtain $\mathbf{V}_2$, $\mathbf{V}_3$, ..., and $\mathbf{V}_n$. In summary, we achieve the fast algorithm for calculating the potential, denoted as Algorithm 2.

Algorithm 1: Fast matrix-vector multiplication $\mathbf{B}_m\mathbf{v} = \mathbf{z}$.

Step 1: Compute z_1 by using $z_1 = (2+2h)v_1 - hv_2$;
Step 2: Cycle computing z_j by using $z_j = (-h)v_{j-1} + (2+2h)v_j - hv_{j+1}$, $j = 2,\ldots,m-1$;
Step 3: Compute z_m by using $z_m = (-h)v_{m-1} + (2+h)v_m$.

As is well-known, the computational complexity of vector multiplication for the tridiagonal quasi-Toeplitz matrix is $O(m)$, which corresponds to the computational complexity of Algorithm 1. Furthermore, the computational complexity of DST-VI is $O(m\log_2 m)$ [28, 29]. Furthermore, during the recursive computation, Algorithm 1 is nested, resulting in a computational complexity of $O(mn)$ at this stage. Considering the above analysis, the computational complexity of the computational potential for Algorithm 2 is $O(m\log_2 m) + O(mn)$.

Algorithm 2: Fast algorithm for computing $U_{m\times n}(x,y)/J$.

Step 1: Compute ϖ_j by using Eq. (14), $j = 1,2,\ldots,m$;
Step 2: Compute $\cosh(\sigma_j) = \frac{\varpi_j}{2}$, $j = 1,2,\ldots,m$;
Step 3: Compute $T_k^{(j)}$ and k by using Eq. (13);
Step 4: Compute $L_0^{(j)}$ and $L_1^{(j)}$ by using Eq. (46), $j = 2,\ldots,m$;
Step 5: Compute $\mathbf{V}_k$ by $\mathbf{L}_0$, $\mathbf{L}_1$, Eq. (43) and DST-VI, $k = 0,1$;
Step 6: Compute $\mathbf{B}_m\mathbf{V}_k$ by using Algorithm 1, $k = 1,2,\ldots$;
Step 7: Cycle computing $\mathbf{V}_k$ by using Eq. (38), $k = 2,3,\ldots$;
Step 8: Compute $U_{m\times n}(x,y)/J$ by using Eq. (15).

Below, we provide two examples of calculating potential using the fast Algorithm 2.

Example 1 In the fan resistor network, we consider the following parameters: $m = 800$, $n = 10$, $x_1 = 2$, $y_1 = 300$, $x_2 = 8$, $y_2 = 500$, $r = r_1 = r_2 = 1$, and $r_0 = 100$. Our objective is to solve for $U_{800\times10}(x,y)/J$ each node, as illustrated in Fig. 8.

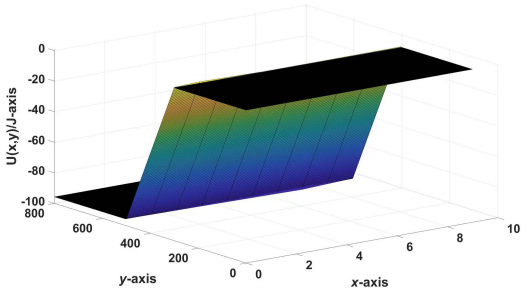

Fig. 8: A scatterplot of $U_{800\times10}(x,y)/J$ calculated by the Algorithm 2.

Example 2 Consider $m = 1200$, $n = 10$, $x_1 = 3$, $y_1 = 500$, $x_2 = 9$, $y_2 = 800$, $r = r_1 = r_2 = 1$, and $r_0 = 100$. The potential at each node is calculated using the fast Algorithm 2, and $U_{1200\times10}(x,y)/J$ is displayed in Fig. 9.

CALCULATING EFFICIENCY AND SCALE OF POTENTIALS

In this section, we utilize the APFs (1) and (8), along with the fast Algorithm 2, to calculate the potential of the fan resistor network. The objective is to compare

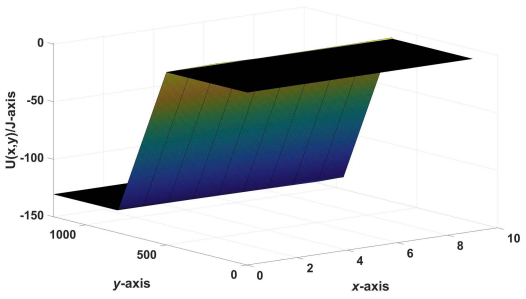

Fig. 9: A scatterplot of $U_{1200\times10}(x,y)/J$ calculated by the Algorithm 2.

Table 1: The time taken to calculate the potential using APFs (1) and (8), respectively, where $r = r_0 = 1$.

$m\times n$	(x_1,y_1)	(x_2,y_2)	r/r_0	t_1	t_2
50×50	(20, 20)	(40, 40)	1	0.0609	0.0388
100×100	(20, 20)	(100, 100)	1	0.3268	0.1355
220×220	(20, 20)	(100, 100)	1	–	0.7861
300×300	(20, 20)	(100, 100)	1	–	1.7325
400×400	(20, 20)	(100, 100)	1	–	9.8072
500×500	(20, 20)	(100, 100)	1	–	–

each method's computational scale and time required. The calculation scale in this experiment is denoted by $m\times n$, representing the potential between $d(x,y)$ ($0\leqslant x\leqslant m$, $1\leqslant y\leqslant n$) and the origin O. The time taken to compute the potential using the APFs (1) and (8), as well as the fast Algorithm 2, are denoted by t_1, t_2, and t_3 respectively. The time is measured in seconds, and "–" signifies that the calculation scale or time exceeds 4000 seconds.

The experiment is conducted on an AMD Ryzen 9 5900HX CPU (3.30 GHz, 8 cores, 16 threads) and an NVIDIA GeForce RTX 3080 Laptop GPU (16 GB VRAM). Matlab R2018b completes the experiment within a Windows 11 operating system. When $r_1 = r_2 = 1$, different values of r and r_0 (i.e., r/r_0) are employed to conduct the experiment.

Remark 4 In Tables 1, 2, and 3, it is evident that under the same conditions, the size and efficiency of calculating the potential using the APF (8) is significantly enhanced compared with the APF (1). Furthermore, the value of r/r_0 significantly affects the scale of the calculated potential. When the value of r/r_0 decreases, the scale of the potential that can be calculated increases. Conversely, when the value of r/r_0 increases, the scale of the potential that can be calculated decreases.

Table 2: The time taken to calculate the potential using the APFs (1) and (8), respectively, where $r = 1$ and $r_0 = 10$.

$m\times n$	(x_1,y_1)	(x_2,y_2)	r/r_0	t_1	t_2
400×400	(20, 20)	(100, 100)	0.1	18.6334	8.8603
580×580	(20, 20)	(100, 100)	0.1	53.9739	25.1305
700×700	(20, 20)	(100, 100)	0.1	–	41.5562
900×900	(20, 20)	(100, 100)	0.1	–	93.2445
1100×1100	(20, 20)	(100, 100)	0.1	–	185.4651
1200×1200	(20, 20)	(100, 100)	0.1	–	–

Table 3: The time taken to calculate the potential using APFs (1) and (8), respectively, where $r = 1$, $r_0 = 100$.

$m\times n$	(x_1,y_1)	(x_2,y_2)	r/r_0	t_1	t_2
1100×1100	(20, 20)	(100, 100)	0.01	361.5467	194.1443
1500×1500	(20, 20)	(100, 100)	0.01	913.5753	510.1261
1800×1800	(20, 20)	(100, 100)	0.01	–	869.5738
2100×2100	(20, 20)	(100, 100)	0.01	–	1401.8866
2400×2400	(20, 20)	(100, 100)	0.01	–	2098.0369
2400×2500	(20, 20)	(100, 100)	0.01	–	2324.4338

Table 4: The time taken to calculate the potential using APFs (1), (8) and fast Algorithm 2, respectively, where $r = r_0 = 1$.

$m\times n$	$d_1(x_1,y_1)$	$d_2(x_2,y_2)$	t_1	t_2	t_3
500×10	(3, 200)	(8, 400)	0.7855	0.4346	0.0391
1000×10	(3, 200)	(8, 400)	2.6618	1.2789	0.0671
5000×10	(3, 200)	(8, 400)	55.4897	19.7573	0.6831
10000×10	(3, 200)	(8, 400)	215.6189	71.6058	2.2514
50000×10	(3, 200)	(8, 400)	–	3618.1504	49.2791

Remark 5 The significantly improved efficiency of the fast Algorithm 2 in calculating the potential is evident from the data presented in Table 4. Compared to the APFs (1) and (8), the fast Algorithm 2 demonstrates significantly higher efficiency. Furthermore, both the fast Algorithm 2 and the APF (8) can handle larger calculation scales compared to the APF (1).

Conclusion

This paper enhances the APF of the $m\times n$ fan resistor network [23] by utilizing CPs of the second class. Moreover, it presents APFs for specific cases and showcases the potential through a three-dimensional visualization. A fast algorithm based on the DST-VI is developed to compute the potential efficiently. We conducted experiments to analyze and compare the efficiency and scalability of computing the potential using the APFs (1), (8), and the fast algorithm, respectively. The experiments demonstrate that the improved APF (8) expands the computational scale, while the fast algorithm enhances computation efficiency. Finally, this work enhances the efficiency and scale of calculating the potential energy of resistor network.

Acknowledgements: The research was Supported by the National Natural Science Foundation of China (Grant Nos. 12101284 and 12001257), the Natural Science Foundation of Shandong Province (Grant Nos. ZR2020MA051 and ZR2020QA035).

REFERENCES

1. Hadad Y, Soric JC, Khanikaev AB, Alù A (2018) Self-induced topological protection in nonlinear circuit arrays. *Nat Electron* **1**, 178–182.
2. Zhang D, Yang B, Jin YB, Xiao B, Xian G, Xue XL, Li Y (2021) Impact damage localization and mode identification of CFRPs panels using an electric resistance change method. *Compos Struct* **276**, 114587.
3. Kirchhoff G (1847) Ueber die Aufölsung der Gleichungen, auf welche man bei der Untersuchung der linearen Vertheilung galvanischer Ströme geführt wird. *Ann Phys* **148**, 497–508.
4. Winstead V, Demarco CL (2012) Network essentiality. *IEEE T Circuits I* **60**, 703–709.
5. Kirkpatrick S (1973) Percolation and conduction. *Rev Mod Phys* **45**, 497–508.
6. Pennetta C, Alfinito E, Reggiani L, Fantini F, DeMunari I, Scorzoni A (2004) Biased resistor network model for electromigration failure and related phenomena in metallic lines. *Phys Rev B* **70**, 174305.
7. Wu FY (2004) Theory of resistor networks: the two-point resistance. *J Phys A Math Gen* **37**, 6653.
8. T zeng WJ, Wu FY (2006) Theory of impedance networks: the two-point impedance and LC resonances. *J Phys A Math Gen* **39**, 8579.
9. Essam JW, Wu FY (2008) The exact evaluation of the corner-to-corner resistance of an $M \times N$ resistor network: asymptotic expansion. *J Phys A Math Theor* **42**, 025205.
10. Izmailian NS, Kenna R, Wu FY (2014) The two-point resistance of a resistor network: a new formulation and application to the cobweb network. *J Phys A Math Theor* **47**, 035003.
11. Tan ZZ (2015) Recursion-transform method to a non-regular $m \times n$ cobweb with an arbitrary longitude. *Sci Rep* **5**, 11266.
12. Tan ZZ, Essam JW, Wu FY (2014) Two-point resistance of a resistor network embedded on a globe. *Phys Rev E* **90**, 012130.
13. Essam JW, Tan ZZ, Wu FY (2014) Resistance between two nodes in general position on an $m \times n$ fan network. *Phys Rev E* **90**, 032130.
14. Tan ZZ (2017) Recursion-transform method and potential formulae of the $m \times n$ cobweb and fan networks. *Chin Phys B* **26**, 090503.
15. Tan Z, Tan ZZ (2018) Potential formula of an $m \times n$ globe network and its application. *Sci Rep* **8**, 9937.
16. Tan ZZ, Tan Z (2020) Electrical properties of an arbitrary $m \times n$ rectangular network. *Acta Phys Sin* **62**, 020502.
17. Tan ZZ (2022) Resistance theory for two classes of n-periodic networks. *Eur Phys J Plus* **137**, 1–12.
18. Zhou YF, Zheng YP, Jiang XY, Jiang ZL (2022) Fast algorithm and new potential formula represented by Chebyshev polynomials for an $m \times n$ globe network. *Sci Rep* **12**, 21260.
19. Jiang ZL, Zhou YF, Jiang XY, Zheng YP (2023) Analytical potential formulae and fast algorithm for a horn torus resistor network. *Phys Rev E* **107**, 044123.
20. Jiang XY, Zhang GJ, Zheng YP, Jiang ZL (2024) Explicit potential function and fast algorithm for computing potentials in $\alpha \times \beta$ conic surface resistor network. *Expert Syst Appl* **238**, 122157.
21. Zhou YF, Jiang XY, Zheng YP, Jiang ZL (2023) Exact novel formulas and fast algorithm of potential for a hammock resistor network. *AIP Adv* **13**, 095127.
22. Zhao WJ, Zheng YP, Jiang XY, Jiang ZL (2023) Two optimized novel potential formulas and numerical algorithms for $m \times n$ cobweb and fan resistor networks. *Sci Rep* **13**, 12417.
23. Tan Z, Tan ZZ, Chen J (2018) Potential formula of the nonregular $m \times n$ fan network and its application. *Sci Rep* **8**, 5798.
24. Mason JC, Handscomb DC (2002) *Chebyshev Polynomials*, Chapman & Hall/CRC, New York, NY.
25. Udrea G (1996) A note on the sequence $(W_n)_{n \geqslant 0}$ of A.F. Horadam. *Port Math* **53**, 143–156.
26. Garcia SR, Yih S (2018) Supercharacters and the discrete Fourier, cosine, and sine transforms. *Commun Algebra* **46**, 3745–3765.
27. Sanchez V, Garcia P, Peinado AM, Segura JC, Rubio AJ (1995) Diagonalizing properties of the discrete cosine transforms. *IEEE T Signal Process* **43**, 2631–2641.
28. Liu Z, Chen S, Xu W, Zhang Y (2019) The eigenstructures of real (skew) circulant matrices with some applications. *Comput Appl Math* **38**, 178.
29. Yip PC, Rao KR (1985) DIF algorithms for DCT and DST. In: *IEEE Int Conf on Acoustics, Speech, and Signal Processing (ICASSP'85)*, Tampa, FL, pp 776–779.